



Short communication

High efficiency flexible dye-sensitized solar cells by multiple electrophoretic depositions

Wei-Hao Chiu^a, Kun-Mu Lee^c, Wen-Feng Hsieh^{a,b,*}^a Department of Photonics, Institute of Electro-Optical Engineering, National Chiao Tung University, 1001 Tahsueh Road, Hsinchu 30050, Taiwan^b Institute of Electro-Optical Science and Engineering, National Cheng Kung University, Tainan, Taiwan^c Green Energy and Environment Research Laboratories, Industrial Technology Research Institute, Hsinchu 310, Taiwan

ARTICLE INFO

Article history:

Received 26 October 2010

Received in revised form

14 December 2010

Accepted 16 December 2010

Available online 24 December 2010

Keywords:

Electrophoretic deposition (EPD)

Titanium dioxide (TiO₂)

Dye-sensitized solar cells (DSCs)

Low-temperature fabrication

Photovoltaics

ABSTRACT

A multiple electrophoretic deposition (EPD) of binder-free TiO₂ photoanode has been developed to successfully fill the crack occurring after air-drying on the first EPD-TiO₂ film surface. With the slow 2nd EPD, high quality TiO₂ thin films are acquired on flexible ITO/PEN substrates at room temperature and the device efficiency of the dye-sensitized solar cell achieved 5.54% with a high fill factor of 0.721. Electrochemical impedance spectroscopy measurements analyze the great enhancement of the photovoltaic performance through multiple EPD. The electron diffusion coefficient improved by about 1 order of magnitude in crack-less multiple-EPD TiO₂ films. With the scattering layer, the device reveals a high conversion efficiency of up to 6.63% under AM 1.5 G one sun irradiation, having a short circuit current density, open circuit voltage, and filling factor of 12.06 mA cm⁻², 0.763 V and 0.72, respectively.

Crown Copyright © 2010 Published by Elsevier B.V. All rights reserved.

1. Introduction

During the past decade, dye-sensitized solar cells (DSCs) [1] are one of the potential photovoltaic (PV) devices due to low-cost production with simple materials and manufacturing equipments, potentially flexible device applications, and high light-to-energy conversion efficiency. It has currently achieved more than 11.5% efficiency [2]. The DSCs consist of several parts, including a nanocrystalline electron-transporting network made of wide-band gap semiconductors such as TiO₂ and ZnO, covered with a monolayer dye with high molar extinction, electrolyte film as hole transport material, and counter electrode.

As the dye molecules absorb light, the photon-generated electrons are injected from the excited dyes into the mesoporous semiconductor network and transported to the transparent conducting oxides (TCOs) on the glass or flexible substrate. On the other side, the electrolyte filled in the pores of porous semiconductor network acts as redox couples (usually I₂/I₃⁻) to regenerate the oxidized dyes and connect to the counter electrode, such as Pt, carbon

[3], and polymer [4]. Each component in DSCs plays an important role in achieving high photon-to-electric conversion efficiency.

Nowadays, studying the light-weight flexible DSCs is an important issue because of the applications in powering mobile devices such as laptop computers, and mobile phones. The fluorine-doped tin oxide (FTO) glass substrate has been replaced by the light-weight substrates that can be categorized into polymer substrate such as polyethylene naphthalate coated with indium-doped tin oxide (ITO/PEN) [5] and metal substrate such as Ti [6] and stainless [7]. Although high-temperature sintering of the metal substrate can improve the connection of TiO₂ nanoparticles (NPs), the back-side illumination of DSCs with metal substrate has lowered the IPCE response in the wavelength range of 540–680 nm because of the absorption of the electrolytes [6]. The polymer substrate is a candidate for flexible DSCs, but requires a fabrication process designed in a temperature range below 150 °C. These flexible DSCs achieved a conversion efficiency of 4.1% with 100 mW cm⁻² illumination [5]. Hagfeldt et al. [8] introduced a new method to prepare the TiO₂ photoanode at room temperature (RT), obtaining an overall conversion efficiency of 5.2% under 0.1 sun irradiation. Cheng et al. proposed a low-temperature chemically sintered process to achieve a 5% plastic-based DSCs, under 1 sun (100 mW cm⁻²) [9]. In 2010, Arakawa et al. reported the plastic-substrate DSCs with conversion efficiency (η) > 7% by optimizing the compress conditions, the thickness of the TiO₂ layer, and the surface treatment of the plastic-substrate [10]. Furthermore, by maintaining the original

* Corresponding author at: Department of Photonics, Institute of Electro-Optical Engineering, National Chiao Tung University, Rm No. 210, CPT Building, 1001 Tahsueh Road, Hsinchu 30050, Taiwan. Tel.: +886 3 5712121x56316; fax: +886 3 5716631.

E-mail address: wfhshieh@mail.nctu.edu.tw (W.-F. Hsieh).

electrical property, a lift-off process has been proposed to transfer pre-sintered porous layers to an arbitrary second substrate [11].

Many studies have explored the preparation of various semiconductor photoanodes at low temperatures. Nanotubular TiO₂ grown by Ti anodization was tested as the photoanode for DSCs [12,13]. In ZnO-based DSCs, hydrothermal-growth 1D structure, such as nanowires, was also performed [14,15]. However, due to the smaller photoanode surface area with the lower dye loading, most of these 1D-nanostructured DSCs have lower current density than those made by NPs. In the low-temperature fabricated DSCs, nanoparticles remain widely used and the methods of depositing NPs on the substrate have been reported doctor-blade coating [16], spray coating [17] and electrophoretic deposition (EPD) [5]. The EPD is a concerned technique in which charged NPs in a suspension that includes additives and solvent move toward an oppositely charged electrode, depositing themselves onto a substrate under an applied DC electric field. Because of the fast deposition rate with no restriction on the substrate shape, this binder-free technology may mass produce any substrate. Much research has reported using EPD to prepare TiO₂ films for DSCs. Miyasaka and Kijitori [5] fabricated DSCs at low temperature with EPD-TiO₂ film, obtaining 4.3% efficiency with an incident solar irradiance of 23 mW cm⁻². However, when the EPD-TiO₂ films dry at room temperature, the micro-cracks (μ -cracks) occur at the film surface to degrade the DSC performance [18,19]. To reduce the μ -cracks of TiO₂ film and minimize the crack problems, the mixture suspension of TiO₂ and MWCNTs (multi-wall carbon nanotubes) has been deposited on FTO glass [20].

In this article, a multiple EPD reduces the cracks occurring upon drying of the first EPD-TiO₂ film to enhance the efficiency at RT. The surface morphology was studied by scanning electron microscopy (SEM) and related DSC performances were discussed. The electrochemical impedance spectroscopy (EIS) analyzed and correlated the film quality with the electron diffusion dynamics of DSCs.

2. Experimental detail

P-90 TiO₂ nanoparticles (a kind gift from Degussa AG, Germany), isopropyl alcohol (IPA), acetonitrile (ACN, HPLC grade, J.T. Baker), methoxypropionitrile (MPN, Alfa Aesar), tert-butyl alcohol (t-BuOH), iodine 99.8% (I₂, Aldrich), tetrabutylammonium iodide (TBAI), N-methylbenzimidazole (NMBI, Aldrich), and anhydrous lithium iodide (LiI, Merck) were used as received without further purification. The ruthenium complex dye cis-bis(isothiocyanato)bis(2,2'-bipyridyl-4,4'-dicarboxylato)-ruthenium(II) bis-tetrabutylammonium, commonly termed N719, was purchased from Solaronix (Aubonne, Switzerland). Indium tin oxide (ITO)-coated polyethylene naphthalate (PEN) (10 Ω per square, thickness 120 μ m) was purchased from Tobe, Inc. Through sol-gel growth in a basic solution, the scattered TiO₂ NPs with ca. 100 nm diameter were synthesized. Mixing 58.6 g titanium isopropoxide with 290 mL distilled water yielded a colloidal suspension which was then filtered and placed in an autoclave containing 20 mL tetramethylammonium hydroxide (TMAH) at 250 °C for 12 h. Finally, the solution in the autoclave was washed by DI water and centrifuged.

ITO/PEN substrates were cleaned with mild soap and ethanol, thoroughly rinsed with deionized water (18.2 M Ω), then dried by a clean air stream. EPD used the flexible TiO₂ photoanode as the transparent conductive substrate for the plastic TiO₂ electrode. The TiO₂ suspension for EPD consisted of 0.25 g TiO₂ in 100 mL IPA, and stirred with a magnetic stirrer overnight; it was ultrasonically dispersed for 1.5 h before adding into the electrophoretic cell. The two electrophoretic electrodes of fluorine-doped tin oxide (F:SnO₂, FTO) conductive glass, and ITO/PEN film were separated by 1.5 cm,

and served as the cathode and anode electrode, respectively. A Keithley 2400 Source Meter was applied as a power supply for different currents and deposition durations at the constant current mode which was more effective and controllable than the constant voltage mode [21]. After drying TiO₂-deposited ITO/PEN substrate at RT and one atmospheric pressure, 100 MPa pressure treatment enhanced the photovoltaic performance of the device (see [supplementary information](#)).

The mesoporous TiO₂ photoanode was immersed in a solution of 0.5 mM N719 dye solution in ACN/t-BuOH (v/v = 1:1) binary solvent at 40 °C for 4 h to adsorb sufficient N719 dye for light harvesting. To remove the remaining dye, the dye-sensitized photoanode was rinsed with ACN, and dried under atmosphere condition at RT. A platinum-sputtered ITO/PEN film served as the counter electrode. A two-electrode sandwich cell separated by 60 μ m spacer (Surlyn) was filled with an electrolyte consisting of 0.4 M LiI, 0.4 M tetrabutylammonium iodide (TBAI), 0.04 M I₂ and 0.5 M N-methylbenzimidazole (NMBI) in ACN/MPN mixture (v/v = 1:1).

In using a black mask, the effective working area of the device is typically about 0.238 cm². For current-voltage characteristics and electrochemical impedance spectroscopy (EIS) measurements, a white light source (Yamashita Denso, YSS-100A) provided an irradiance of 100 mW cm⁻² (equivalent to one sun at AM 1.5) on the surface of the solar cell, and an electrochemical analyzer collected the data (Autolab, PGSTAT3) at 25 °C. Using a silicon photodiode (BS-520, Bunko Keiki), the light power was calibrated with a set of neutral density filters. Impedance measurements were performed with a computer-controlled electrochemical analyzer (Autolab, PGSTAT3). The forward bias that set for the open circuit voltage with an AC amplitude of 10 mV was applied between the photoanode and counter electrode, and the explored frequency range ranged from 50 mHz to 1 MHz. An IPCE measurement system (C-995, PV-measurement Inc.) measured the action spectra of the incident monochromatic photon to current conversion efficiency (IPCE) for solar cells. A halogen lamp (500 W) light source served as an additional light bias. And due to the capacitance effect of the DSCs [22], the chopper frequency was set to 4 Hz.

3. Results and discussion

For low-temperature fabricated DSCs especially by EPD, the volatile organic compounds such as isopropyl alcohol (IPA), methanol, or ethanol were the solvent of the binder-free suspension or paste. Cracks in the film would constantly occur after air-drying that degraded the device performance. We applied one-step and two-step EPDs separately in this experiment to deposit P-90 TiO₂ NPs onto ITO/PEN flexible substrates. For one-step EPD, we applied a constant current density of 20 μ A cm⁻² for 5 min; whereas, two-step EPD was performed twice for 2.5 min with the same conditions but via air-drying the sample between the steps. The charge density in EPD stayed constant in these two processes.

Fig. 1 shows the surface morphology examined by an optical microscope, illustrating the interconnected P-90 TiO₂ NPs thin film. Huge microcracks in the one-step process deposited films (Fig. 1a) are wider and deeper than those of the two-step ones (Fig. 1b). These results suggest that the 2nd EPD could fill the cracks produced in the 1st EPD to form a better quality microstructure photoanode. To understand the role of thin films made by the one-step and two-step EPDs in DSC devices, three photoanodes for each method were prepared and assembled into DSC devices, whose performances are listed in Table 1. Because the same deposition charges density of 6 mC cm⁻² prepared all DSCs, we obtained a similar thickness of 5 μ m with almost the same J_{SC} and V_{OC} of about 8.94 mA cm⁻² and 0.784 V. However, slightly improving the fill-factor (FF) from 0.595 to 0.690 for the one made of two-step

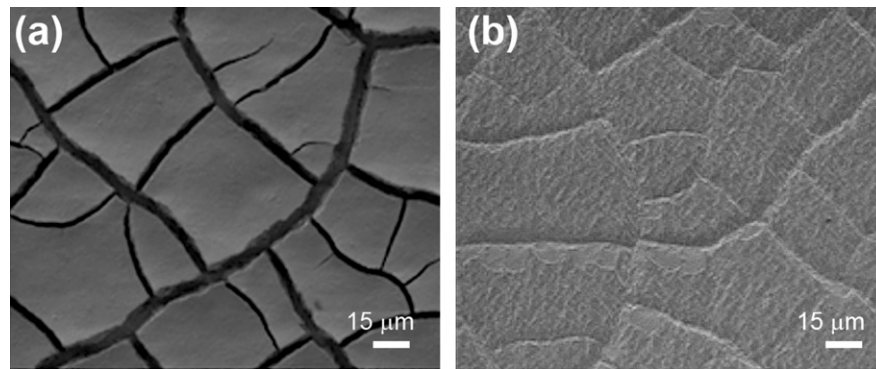


Fig. 1. The microscopy pictures of electrophoretically deposited P-90 TiO₂ nanostructure on ITO/PEN film by one-step process (a) and two-step process (b).

Table 1

Dye-sensitized solar cell performances with one-step or two-step EPD preparation methods. All photoanodes were compressed by 100 MPa pressure before device assembling.

Method	Process EPD current density [time] ($\mu\text{A cm}^{-2}$ [min])	J_{SC} (mA cm^{-2})	V_{OC} (V)	FF	η (%)
One-step	20 [5]	8.81	0.780	0.595	4.09
Two-step	20 [2.5] + 20 [2.5]	8.94	0.784	0.690	4.83

EPD may explain the fewer cracks of EPD film. In this plastic-based DSC with two-step EPD photoanode, we achieved a conversion efficiency of 4.83%. The two-step EPD photoanode has better film quality to improve the DSC device efficiency.

In order to enhance the dye absorption and increase the thickness of the mesoporous photoanode made by EPD, we increased the total deposition charge density from 6 to 12 mC cm^{-2} . Meanwhile, to clarify the effect of the device performance by different deposition rates, we varied the EPD current density from 20 to 5 $\mu\text{A cm}^{-2}$. Table 2 provides the performance data of various DSCs. By increasing the applied EPD current density, the deposition thickness, as expected, increases from 5 to 20 $\mu\text{A cm}^{-2}$. The higher applied EPD current density causes the higher internal EPD voltage (or electric field), thus, the TiO₂ NPs in the solvent could easily overcome the gravity and friction force of the solvent. In contrast with the V_{OC} , J_{SC} increases with the TiO₂-film thickness because the more photoanode surface area with the thicker film not only enhances the dye loading but also creates more inhomogeneous light intensity in the film, decreasing the effective Fermi level of TiO₂ photoanode.

The DSCs with the slowest deposition rate (5 $\mu\text{A cm}^{-2}$; 20 min) have the highest filling factor of 0.71. This result suggests that the slower deposition rate, the better quality of TiO₂ photoanode is – although the most efficient DSCs with a conversion efficiency of 5.13% was obtained using a two-step EPD with current density of 20 $\mu\text{A cm}^{-2}$ for 5 min in each step. The reason is because thicker TiO₂ film provides a larger area for dye adsorption.

The cracks produced in the 1st EPD film could be filled in the 2nd EPD and the larger applied current density provides the faster deposition rate. We therefore further prepared the DSCs with three deposition rates for the 2nd TiO₂ EPD, i.e. 20 $\mu\text{A cm}^{-2}$; 5 min, 10 $\mu\text{A cm}^{-2}$; 10 min, and 5 $\mu\text{A cm}^{-2}$; 20 min, but with the same 1st EPD condition (20 $\mu\text{A cm}^{-2}$; 5 min). Fig. 2 shows the current density–voltage (J – V) curves of these three devices. Inset table sum-

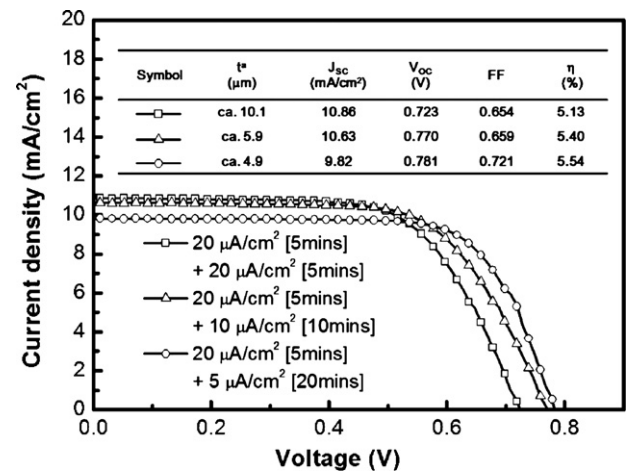


Fig. 2. The effect of different 2nd EPD TiO₂ photoanodes on J – V curve of DSCs. Inset table shows the detail photovoltaic parameters under AM 1.5 G one sun irradiation. ^a The symbol t stands for the TiO₂ film thickness after 100 MPa pressure.

marizes the corresponding thickness (t) of TiO₂ film after 100 MPa pressure, short-circuit current (J_{SC}), open-circuit voltage (V_{OC}), fill factor (FF), and solar-to-electricity conversion efficiency (η).

Although we maintained the same product of current density and deposition time in the three samples, the results reveal quite large difference in film thickness. The slowest deposition rate for a 4.9 μm thick device and the fastest deposition rate for 10.1 μm one indicates that the cracks produced after drying the 1st EPD film may have been filled up more at the slow EPD rate than at the fast rate; therefore the thickness of TiO₂ film is not linearly proportionate to the 2nd EPD rate. With increasing photoanode thickness from 4.9 to

Table 2

Dye-sensitized solar cell performances with two-step EPD preparation methods by various EPD current and time.

Process EPD current density [time] ($\mu\text{A cm}^{-2}$ [min])	t^a (μm)	J_{SC} (mA cm^{-2})	V_{OC} (V)	FF	η (%)
20 [5] + 20 [5]	ca. 10.1	10.86	0.723	0.654	5.13
10 [10] + 10 [10]	ca. 6.8	10.11	0.751	0.646	4.92
5 [20] + 5 [20]	ca. 5.2	8.45	0.781	0.710	4.68

^a TiO₂ film thickness after 100 MPa pressure.

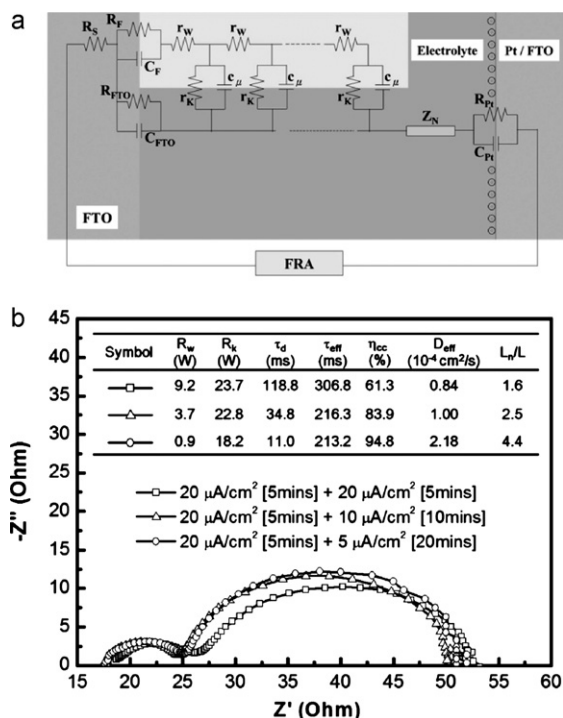


Fig. 3. (a) Transmission line impedance model for typical DSCs, (b) Nyquist plots of DSCs device with the different 2nd EPD TiO₂ photoanodes at V_{OC} under AM 1.5 G one-sun irradiation. The detail fitting parameters of photoanode were listed in inset table.

10.1 μm, V_{OC} decreases from 0.781 V to 0.723 V, whereas, J_{SC} mainly ascribed to the enlargement of the surface area for dye adsorption. The fastest deposited (thickest) DSC is only 1 mA cm⁻² larger than that of the slowest (thinnest) deposited one. We acquired maximal FF of 0.721 and a conversion efficiency of 5.54% for the DSC fabricated with the slowest 2nd deposition rate (5 μA cm⁻²).

To investigate the interfacial charge transfer processes occurring in the each component of DSCs, the electrochemical impedance spectroscopy (EIS), such as the photoanode, electrolyte, and Pt counter electrode [23,24], has been used widely. Fig. 3 compares the Nyquist plots of the DSCs with different 2nd EPD rates which were analyzed and fitted with the well-known transmission-line impedance model (Fig. 3a) of our previous studies [25,26]. The EPD-TiO₂ photoanodes are characterized by the chemical capacitance C_μ, the transport resistance R_W and the TiO₂/electrolyte interfacial charge-transfer resistance (or the so-called recombination resistance), R_k. R_s and Z_N stand for the charge transport resistance of FTO, including external circuits and the finite Warburg impedance in the electrolyte. R_{Pt} and C_{Pt} are the charge-transfer resistance and the capacitance at the Pt surface. R_{FTO} and C_{FTO} are the charge-transfer resistance and the interfacial capacitance at the FTO/electrolyte interface. R_F and C_F are the resistance and the capacitance at the FTO/TiO₂ interface. In the measured frequency range over 50 mHz to 1 MHz, two semicircles of the Nyquist plots were observed clearly. The 1st semicircle (in the kHz range) typically stands for the behavior of the Pt counter electrode, and the 2nd semicircle, determined by only one parameter, $(\tau_k/\tau_d) = (R_k/R_W)$, represents the impedances related to charge-transfer processes in the TiO₂ photoanode [24].

Inset table of Fig. 3b summarizes the fitting results, suggesting that the charge-transfer resistance (R_W) decreases by about 1 order of magnitude by reducing the 2nd EPD rate of the TiO₂ film from 20 μA cm⁻² to 5 μA cm⁻². The slower 2nd EPD rate provides better fill-in for the cracks formed during drying of the 1st EPD film for more efficient electron transport pathway in the TiO₂

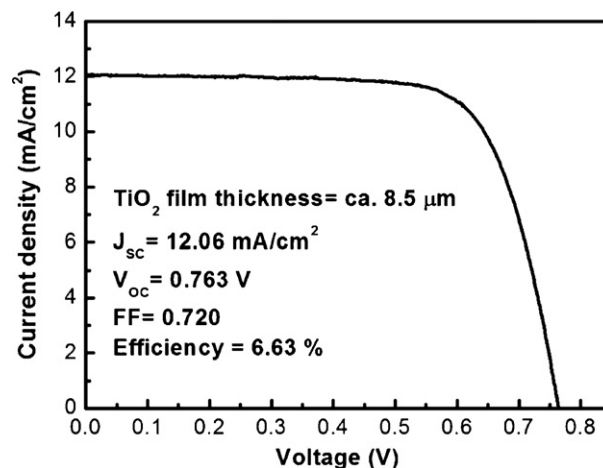


Fig. 4. Photocurrent–voltage characteristics of nanocrystalline TiO₂ photoanode deposited multiply by P-90 and 100 nm NPs measured under AM 1.5 sun irradiation using 0.238 cm² size of black mask.

photoanode. The effective electron lifetime (τ_{eff}), the lifetime of electrons being recombined, and back-injection into the electrolyte is inversely proportional to the fitting peak frequency ($\omega_{max} = 1/\tau_k$) of the 2nd semicircle in the case of $R_k \gg R_W$. The effective electron diffusion time in TiO₂ photoanode (τ_d), given as $\tau_d = \tau_k/(R_k/R_W)$, decreases from 118.8 to 18 ms as the 2nd EPD rate decreases. The effective electron diffusion coefficient in the photoanode (D_{eff}) is calculated using the relation: $D_{eff} = (R_k/R_W)(L^2/\tau_{eff})$, where L is the thickness of photoanode. An efficient D_{eff} of 2.18×10^{-5} cm² s⁻¹ was obtained from the DSC made with the slowest 2nd EPD rate at 5 μA cm⁻². The electron diffusion length expresses the competition between the collection and the recombination of electrons. The effective diffusion length (Ln) can be expressed as $Ln = (D_{eff}\tau_{eff})^{0.5}$. As shown in Fig. 3b, the obtained Ln/L increases about three times by decreasing the 2nd EPD rate from 20 μA cm⁻² to 5 μA cm⁻². All the fitting parameters from EIS analysis indicate that the DSC devices with the higher quality TiO₂ film deposited by the slower deposition rate (5 μA cm⁻²) have more efficient electron transport in the photoanode to achieve a higher conversion efficiency of 5.54%.

Finally, through multiple EPDs, including slow 2nd EPD to completely fill the cracks produced in drying 1st EPD film and the fast-deposited (20 μA cm⁻² deposition current density for 5 min deposition) scattering layer of 100 nm TiO₂ NPs, the scattering layer efficiently scattered sunlight, especially for long wavelengths (see supplementary information). Fig. 4 shows the excellent photovoltaic performance without an antireflection layer under AM 1.5 G one sun irradiation. Its short circuit current density (J_{SC}), open circuit voltage (V_{OC}), and filling factor (FF) are 12.06 mA cm⁻², 0.763 V, and 0.72, respectively, yielding an overall conversion efficiency (η) of 6.63%.

4. Conclusions

Electrophoretic deposition at room temperature and compress treatment prepare TiO₂ thin films on flexible ITO/PEN substrates. The multiple EPDs filled up the cracks caused by drying the previous EPD film and the slow 2nd deposition rate obtained a high conversion efficiency of 5.54%. EIS analyzed the great enhancement of the electron collection which improved the electron diffusion coefficient about 1 order of magnitude in crack-less multiple-EPD TiO₂ films. When the 100 nm TiO₂ NPs were deposited on P-90 EPD film in a DSSC, the device shows the best photovoltaic performance with an energy conversion efficiency of 6.63% due to the 100 nm TiO₂ NPs efficiently scattered sunlight, especially in long wavelength region.

Acknowledgment

The authors acknowledge financial support from the National Science Council of Taiwan (NSC-99-2112-M-006-017-MY3 and NSC-99-2221-E-009-095-MY3), Industrial Technology Research Institute (9301XS6A10), and the Bureau of Energy, Ministry of Economic Affairs (9455DI2110).

Appendix A. Supplementary data

Supplementary data associated with this article can be found, in the online version, at doi:10.1016/j.jpowsour.2010.12.063.

References

- [1] M. Gratzel, *Nature* 414 (2001) 338–344.
- [2] C.Y. Chen, M. Wang, J.Y. Li, N. Pootrakulchote, L. Alibabaei, C.H. Ngoc-le, J.D. Decoppet, J.H. Tsai, C. Gratzel, C.G. Wu, S.M. Zakeeruddin, M. Gratzel, *ACS Nano* 3 (2009) 3103–3109.
- [3] K. Imoto, K. Takahashi, T. Yamaguchi, T. Komura, J. Nakamura, K. Murata, *Solar Energy Materials and Solar Cells* 79 (2003) 459–469.
- [4] K.M. Lee, C.Y. Hsu, P.Y. Chen, M. Ikegami, T. Miyasaka, K.C. Ho, *Physical Chemistry Chemical Physics* 11 (2009) 3375–3379.
- [5] T. Miyasaka, Y. Kijitori, *Journal of the Electrochemical Society* 151 (2004) A1767–A1773.
- [6] S. Ito, N.L.C. Ha, G. Rothenberger, P. Liska, P. Comte, S.M. Zakeeruddin, P. Pechy, M.K. Nazeeruddin, M. Gratzel, *Chemical Communications* (2006) 4004–4006.
- [7] M.G. Kang, N.G. Park, K.S. Ryu, S.H. Chang, K.J. Kim, *Solar Energy Materials and Solar Cells* 90 (2006) 574–581.
- [8] H. Lindstr, A. Holmberg, E. Magnusson, L. Malmqvist, A. Hagfeldt, *Journal of Photochemistry and Photobiology A: Chemistry* 145 (2001) 107–112.
- [9] H.C. Weerasinghe, P.M. Sirimanne, G.V. Franks, G.P. Simon, Y.B. Cheng, *Journal of Photochemistry and Photobiology A: Chemistry* 213 (2010) 30–36.
- [10] T. Yamaguchi, N. Tobe, D. Matsumoto, T. Nagai, H. Arakawa, *Solar Energy Materials and Solar Cells* 94 (2010) 812–816.
- [11] M. Durr, A. Schmid, M. Obermaier, S. Rosselli, A. Yasuda, G. Nelles, *Nature Materials* 4 (2005) 607–611.
- [12] K. Lee, J. Kim, H. Kim, Y. Lee, Y. Tak, D. Kim, P. Schmuki, *Journal of the Korean Physical Society* 54 (2009) 1027–1031.
- [13] D. Kuang, J. Brillet, P. Chen, M. Takata, S. Uchida, H. Miura, K. Sumioka, S.M. Zakeeruddin, M. Gratzel, *ACS Nano* 2 (2008) 1113–1116.
- [14] M. Law, L.E. Greene, J.C. Johnson, R. Saykally, P. Yang, *Nature Materials* 4 (2005) 455–459.
- [15] H.M. Cheng, W.H. Chiu, C.H. Lee, S.Y. Tsai, W.F. Hsieh, *Journal of Physical Chemistry C* 112 (2008) 16359–16364.
- [16] T. Miyasaka, M. Ikegami, Y. Kijitori, *Journal of the Electrochemical Society* 154 (2007) A455–A461.
- [17] M. Okuya, K. Nakade, S. Kaneko, *Solar Energy Materials and Solar Cells* 70 (2002) 425–435.
- [18] J.H. Yum, S.S. Kim, D.Y. Kim, Y.E. Sung, *Journal of Photochemistry and Photobiology A: Chemistry* 173 (2005) 1–6.
- [19] S. Yanagida, A. Nakajima, Y. Kameshima, N. Yoshida, T. Watanabe, K. Okada, *Materials Research Bulletin* 40 (2005) 1335–1344.
- [20] W. Jarernboon, S. Pimanpang, S. Maensiri, E. Swatsitang, V. Amornkitbamrung, *Journal of Alloys and Compounds* 476 (2009) 840–846.
- [21] L. Grinis, S. Dor, A. Ofir, A. Zaban, *Journal of Photochemistry and Photobiology A: Chemistry* 198 (2008) 52–59.
- [22] H. Tian, L. Liu, B. Liu, S. Yuan, X. Wang, Y. Wang, T. Yu, Z. Zou, *Journal of Physics D: Applied Physics* 42 (2009) 5.
- [23] S. Ito, M. Gratzel, F. Fabregat-Santiago, I. Mora-Sero, J. Bisquert, T. Bessho, H. Imai, *Journal of Physical Chemistry B* 110 (2006) 25210–25221.
- [24] M. Adachi, M. Sakamoto, J. Jiu, Y. Ogata, S. Isoda, *Journal of Physical Chemistry B* 110 (2006) 13872–13880.
- [25] W.H. Chiu, C.H. Lee, H.M. Cheng, H.F. Lin, S.C. Liao, J.M. Wu, W.F. Hsieh, *Energy & Environmental Science* 2 (2009) 694–698.
- [26] H.M. Cheng, W.F. Hsieh, *Energy & Environmental Science* 3 (2010) 442–447.